

# Assessment of crystal quality and unit cell orientation in epitaxial $\text{Cu}_2\text{ZnSnSe}_4$ layers using polarized Raman scattering

Christoph Krämmmer,<sup>1,3,\*</sup> Mario Lang,<sup>1,3</sup> Alex Redinger,<sup>2</sup> Johannes Sachs,<sup>1</sup> Chao Gao,<sup>1</sup> Heinz Kalt,<sup>1</sup> Susanne Siebentritt,<sup>2</sup> and Michael Hetterich<sup>1</sup>

<sup>1</sup>*Institute of Applied Physics, Karlsruhe Institute of Technology (KIT), 76131 Karlsruhe, Germany*

<sup>2</sup>*University of Luxembourg, Laboratory for Photovoltaics, Physics and Materials Science Research Unit, L-4422 Belvaux, Luxembourg*

<sup>3</sup>*These authors contributed equally*

\*[christoph.kraemmer@kit.edu](mailto:christoph.kraemmer@kit.edu)

**Abstract:** We use polarization-resolved Raman spectroscopy to assess the crystal quality of epitaxial kesterite layers. It is demonstrated for the example of epitaxial  $\text{Cu}_2\text{ZnSnSe}_4$  layers on GaAs(001) that "standing" and "lying" kesterite unit cell orientations ( $c'$ -axis parallel / perpendicular to the growth direction) can be distinguished by the application of Raman tensor analysis. From the appearance of characteristic intensity oscillations when the sample is rotated one can distinguish polycrystalline and epitaxial layers. The method can be transferred to kesterite layers oriented in any crystal direction and can shed light on the growth of such layers in general.

© 2014 Optical Society of America

**OCIS codes:** (300.6450) Raman spectroscopy, (310.6870) Thin films, other properties.

---

## References and links

1. W. Wang, M. T. Winkler, O. Gunawan, T. Gokmen, T. K. Todorov, Y. Zhu, and D. B. Mitzi, "Device characteristics of CZTSSe thin-film solar cells with 12.6% efficiency," *Adv. Energy Mater.* **4**, 1301465 (2013).
2. S. Oueslati, G. Brammertz, M. Buffière, *Thin Solid Films* (submitted) (2014).
3. A. Redinger, R. Djemour, T. Weiss, J. Sendler, L. Gütay, and S. Siebentritt, "Molecular beam epitaxy of  $\text{Cu}_2\text{ZnSnSe}_4$  thin films grown on GaAs(001)," in *Proceedings of the 39th IEEE Photovoltaics Specialists Conference* (IEEE, 2013), pp.420–426.
4. C. Krämmmer, J. Sachs, M. Lang, L. Pfaffmann, C. Gao, D. Gerthsen, H. Kalt, M. Powalla, and M. Hetterich, "Fabrication of polycrystalline  $\text{Cu}_2\text{ZnSnSe}_4$  layers with strongly preferential grain orientation via selenization of Sn/Cu/ZnSe(001)/GaAs(001) structures," *Appl. Phys. Lett.* **104**, 071913 (2014).
5. S. Siebentritt and S. Schorr, "Kesterites—a challenging material for solar cells," *Prog. Photovoltaics* **20**, 512–519 (2012).
6. S. Ahn, S. Jung, J. Gwak, A. Cho, K. Shin, K. Yoon, D. Park, H. Cheong, and J. H. Yun, "Determination of band gap energy ( $E_g$ ) of  $\text{Cu}_2\text{ZnSnSe}_4$  thin films: On the discrepancies of reported band gap values," *Appl. Phys. Lett.* **97**, 021905 (2010).
7. M. Grossberg, J. Krustok, J. Raudoja, K. Timmo, M. Altosaar, and T. Raadik, "Photoluminescence and Raman study of  $\text{Cu}_2\text{ZnSn}(\text{Se}_x\text{S}_{1-x})_4$  monograins for photovoltaic applications," *Thin Solid Films* **519**, 7403–7406 (2011).
8. M. Altosaar, J. Raudoja, K. Timmo, M. Danilson, M. Grossberg, J. Krustok, and E. Mellikov, " $\text{Cu}_2\text{Zn}_{1-x}\text{Cd}_x\text{Sn}(\text{Se}_{1-y}\text{S}_y)_4$  solid solutions as absorber materials for solar cells," *Phys. Status Solidi A* **205**, 167–170 (2008).
9. R. Djemour, A. Redinger, M. Mousel, L. Gütay, X. Fontané, V. Izquierdo-Roca, A. Pérez-Rodríguez, and S. Siebentritt, "The three A symmetry Raman modes of kesterite in  $\text{Cu}_2\text{ZnSnSe}_4$ ," *Opt. Express* **21**, A695–A703 (2013).

10. R. Djemour, M. Mousel, A. Redinger, L. Güтай, A. Crossay, D. Colombara, P. J. Dale, and S. Siebentritt, "Detecting ZnSe secondary phase in  $\text{Cu}_2\text{ZnSnSe}_4$  by room temperature photoluminescence," *Appl. Phys. Lett.* **102**, 222108 (2013).
11. N. Vora, J. Blackburn, I. Repins, C. Beall, B. To, J. Pankow, G. Teeter, M. Young, and R. Noufi, "Phase identification and control of thin films deposited by co-evaporation of elemental Cu, Zn, Sn, and Se," *J. Vac. Sci. Technol. A* **30**, 051201 (2012).
12. J. J. S. Scragg, L. Choubrac, A. Lafond, T. Ericson, and C. Platzer-Björkman, "A low-temperature order-disorder transition in  $\text{Cu}_2\text{ZnSnS}_4$  thin films," *Appl. Phys. Lett.* **104**, 041911 (2014).
13. M. Guc, S. Levchenko, V. Izquierdo-Roca, X. Fontané, E. Arushanov, and A. Pérez-Rodríguez, "Polarized Raman scattering analysis of  $\text{Cu}_2\text{ZnSnSe}_4$  and  $\text{Cu}_2\text{ZnGeSe}_4$  single crystals," *J. Appl. Phys.* **114**, 193514 (2013).
14. D. Dumcenco and Y.-S. Huang, "The vibrational properties study of kesterite  $\text{Cu}_2\text{ZnSnS}_4$  single crystals by using polarization dependent Raman spectroscopy," *Opt. Mater.* **35**, 419–425 (2012).
15. A. Redinger, D. M. Berg, P. J. Dale, and S. Siebentritt, "The Consequences of Kesterite Equilibria for Efficient Solar Cells," *J. Am. Chem. Soc.* **133**, 3320–3323 (2011).
16. B. Shin, Y. Zhu, N. A. Bojarczuk, S. Jay Chey, and S. Guha, "Control of an interfacial  $\text{MoSe}_2$  layer in  $\text{Cu}_2\text{ZnSnSe}_4$  thin film solar cells: 8.9% power conversion efficiency with a tin diffusion barrier," *Appl. Phys. Lett.* **101**, 053903 (2012).
17. R. Loudon, "The Raman effect in crystals," *Adv. Phys.* **13**, 423–482 (1964).
18. K. Momma and F. Izumi, "VESTA 3 for three-dimensional visualization of crystal, volumetric and morphology data," *J. Appl. Crystallogr.* **44**, 1272–1276 (2011).
19. T. Gürel, C. Sevik, and T. Çağın, "Characterization of vibrational and mechanical properties of quaternary compounds  $\text{Cu}_2\text{ZnSnS}_4$  and  $\text{Cu}_2\text{ZnSnSe}_4$  in kesterite and stannite structures," *Phys. Rev. B* **84**, 205201 (2011).
20. A. Khare, B. Himmetoglu, M. Johnson, D. J. Norris, M. Cococcioni, and E. S. Aydil, "Calculation of the lattice dynamics and Raman spectra of copper zinc tin chalcogenides and comparison to experiments," *J. Appl. Phys.* **111**, 083707 (2012).

## 1. Introduction

In recent years,  $\text{Cu}_2\text{ZnSn}(\text{S},\text{Se})_4$  has attracted increasing attention as a promising candidate for sustainable thin-film photovoltaics. The structural similarity to the well-established  $\text{Cu}(\text{In},\text{Ga})(\text{S},\text{Se})_2$  (CIGS) and the absence of rare materials such as indium might be an important step to sustainable thin-film photovoltaics in the future. However, achieved power-conversion efficiencies of 12.6 % [1] for the sulphoselenide and 10.4 % [2] for the pure  $\text{Cu}_2\text{ZnSnSe}_4$  (CZTSe) are still far below those of CIGS.

One key aspect to further improve the efficiency of CZTSe solar cells is a detailed understanding of the physical properties of this complex material. Optical techniques such as modulation spectroscopy, time-resolved and temperature-dependent photoluminescence are powerful tools to gain insight into the band structure and carrier recombination mechanisms of CZTSe. However, in order to reach their full potential all of these techniques rely on high-quality samples, preferentially single-crystalline and with a low amount of secondary phases.

Epitaxial samples can be fabricated using molecular-beam epitaxy [3] or a two-step approach [4] on GaAs(001). The single crystalline substrate leads to a strong preferential orientation of the growing film. In the case of GaAs(001) the CZTSe layer is also oriented along the (001) orientation in contrast to polycrystalline absorbers grown on molybdenum coated soda lime glass which usually exhibit a dominant 112 peak (JCPDS-52-0868). However, due to the tetragonal kesterite unit cell with a  $c'/2a'$ -ratio of 0.996 ( $a'=5.695 \text{ \AA}$ ,  $c'=11.345 \text{ \AA}$ ) [5] there are three possible orientations when CZTSe is grown epitaxially on a cubic GaAs(001) substrate. One "standing" ( $c'$ -axis  $\parallel$  GaAs[001]) and two "lying" orientations ( $c'$ -axis  $\parallel$  GaAs[100] and GaAs[010], respectively) can be found, the two latter ones being equally probable due to the cubic symmetry of GaAs. The same situation can be found for the sulphide kesterite  $\text{Cu}_2\text{ZnSnS}_4$  when grown on a cubic Si substrate. These different orientations can not be distinguished by X-ray diffraction (XRD).

Raman spectroscopy has already turned out to be a valuable and reliable technique to identify CZTSe by its main phonon modes [6–9] and to discriminate frequently occurring secondary phases such as, e.g.,  $\text{SnSe}_x$  compounds, ZnSe or  $\text{Cu}_2\text{SnSe}_3$  [10, 11].

Still, this technique holds a greater potential than mere phase identification. Using Raman spectroscopy, Scragg *et al.* [12] were able to show the preferential formation of ordered or disordered sulphidic kesterite under different annealing conditions. Guc *et al.* [13] determined the ratios of the elements of a Raman tensor which can be used to describe polarized Raman spectroscopy on CZTSe single crystals and Dumcenco *et al.* [14] studied CZTS samples with polarization-dependent Raman measurements.

Here, we analyze the crystallographic orientation for CZTSe epitaxial layers fabricated by two different techniques outlined below. As discussed in more detail later on, for epitaxially ordered samples the intensity of the CZTSe Raman modes shows a characteristic behaviour when the sample is rotated around the optical axis. This behaviour depends on the kind of phonon mode one is observing but also on the grain orientations within the sample. In the example of CZTSe layers on GaAs(001), we show that the "standing" kesterite unit cell orientation is prevalent and is independent of the fabrication route. Furthermore, the formalism can be transferred to samples with an arbitrary crystallographic orientation.

## 2. Experiments and results

Epitaxial  $\text{Cu}_2\text{ZnSnSe}_4$  layers on GaAs(001) have been fabricated in a molecular-beam epitaxy (MBE) system via coevaporation of Cu, Zn, Sn, SnSe from effusion cells and Se from a valved cracker source at a nominal substrate temperature of 450 °C. The additional SnSe source is used to compensate for SnSe losses during growth [15]. Further details of the growth process can be found in [3]. In an alternative approach, strongly textured CZTSe samples are obtained using a two-step process. A Sn/Cu/ZnSe(001) stack is grown on GaAs(001) using MBE, and is then annealed in a selenium atmosphere. These layers show a strong preferential grain orientation in all three dimensions and can be seen as an intermediate step between real polycrystalline and fully epitaxial samples. Further details on the fabrication as well as the characterization of the samples can be found in [4]. In the following, these samples will be referred to as textured samples. For comparison, polycrystalline CZTSe samples have been fabricated by low-temperature coevaporation of elemental Cu,Zn,Sn and Se onto Mo-coated soda-lime glass (Mo/SLG) in the same MBE system where the precursors for the textured samples have been deposited, followed by selenization in a tube furnace. The process which is used is similar to that reported by Shin *et al.* [16].

Raman spectra are recorded using a frequency-doubled Nd:YVO<sub>4</sub> laser ( $\lambda=532$  nm) in a confocal excitation/detection setup. A double Fresnel rhomb is used to rotate the incoming linear polarization of the laser. Light is focused and scattered light from the sample is then collected using a microscope objective (20×, NA=0.4). The sample itself is mounted on a motorized rotation mount (MRM) and can be rotated around the optical axis ( $\parallel$  GaAs[001] direction). In the following, the corresponding angle of rotation will be referred to as  $\alpha$ . After passing a razor-edge filter followed by a polarizer (analyzer) light is dispersed in a 0.46 m focal length monochromator using a 2400 l/mm grating. The spectra are then recorded using a charge-coupled device (CCD) camera.

Kesterite belongs to the space group  $\bar{I}4$ , and Raman modes of 3 different symmetries—namely A,B and E—are possible. The different Raman tensors for this space group are given in Table 1 [17].

The intensity  $I$  of a Raman mode with a corresponding tensor  $\mathcal{R}$  for incoming light of a given polarization  $\mathbf{e}_i$  and scattered light with a polarization  $\mathbf{e}_s$  is proportional to

$$I \propto |\mathbf{e}_s^T \mathcal{R} \mathbf{e}_i|^2$$

where  $\mathbf{e}_s^T$  denotes the transposed vector. Consequently, the Raman signal for a polarizer configuration  $\mathbf{e}_i \parallel \mathbf{e}_s$  depends on the diagonal elements of the transformed Raman tensor, and for

Table 1. Raman tensors with tensor elements a-f for the space group  $I\bar{4}$  assuming a standing unit cell ( $z'|z \parallel \text{GaAs}[001]$ ) [17]

$$\mathcal{R}_A = \begin{pmatrix} a & 0 & 0 \\ 0 & a & 0 \\ 0 & 0 & b \end{pmatrix} \quad \mathcal{R}_{B(Z)} = \begin{pmatrix} c & d & 0 \\ d & -c & 0 \\ 0 & 0 & 0 \end{pmatrix}$$

$$\mathcal{R}_{E(X)} = \begin{pmatrix} 0 & 0 & e \\ 0 & 0 & f \\ e & f & 0 \end{pmatrix} \quad \mathcal{R}_{E(Y)} = \begin{pmatrix} 0 & 0 & f \\ 0 & 0 & -e \\ f & -e & 0 \end{pmatrix}$$

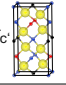
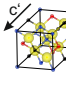
$\mathbf{e}_i \perp \mathbf{e}_s$  the signal is represented by off-diagonal tensor elements. The different possible kesterite unit cell orientations can now be considered by applying the appropriate rotation matrices. For example, the Raman tensors  $\mathcal{R}_A$  of the two lying unit cells are obtained by applying a rotation around the x- and y-axis of the laboratory system and are given by  $\text{diag}(a, b, a)$  and  $\text{diag}(b, a, a)$ . The Raman tensors for B- and E-modes can be treated analogously. Again, it is important to note that the two possible lying kesterite unit cell orientations on GaAs(001) must occur simultaneously due to the cubic structure of the substrate. In contrast, the lattice mismatch and the formation energy are slightly different for standing and lying kesterite due to the  $c'/2a'$  ratio of 0.996 of the CZTSe unit cell. The intensity dependence of the Raman signal for a sample rotation around the optical axis can be described by a transformation of the Raman tensors using matrices for the rotation around the laboratory z-axis. Table 2 summarizes the resulting intensity dependencies on the rotation angle  $\alpha$  for Raman modes of different symmetry and the two different polarizer configurations for a given set of tensor elements a-f (Unit cell pictures created using *VESTA3* [18]).

For the lying kesterite the intensity contributions from both orientations add up to the resulting signal. Despite their mathematical complexity, all trigonometric expressions in Table 2 describe oscillations with a characteristic period of  $90^\circ$  which essentially results from the symmetry of the CZTSe unit cell. At this point, it is important to mention that a single lying unit cell orientation would result in an oscillation with a period of  $180^\circ$  in the A and B-mode for  $\mathbf{e}_i \parallel \mathbf{e}_s$  due to the reduced symmetry along the optical axis. However, the second lying unit cell yields the same oscillations but shifted by  $90^\circ$  relative to the first orientation. In the end the coexistence of both lying configurations results in an oscillation with an effective period of  $90^\circ$ . This means that all the oscillations described in Table 2 exhibit the same period of  $90^\circ$  and are further in phase for one particular polarizer configuration. Furthermore, the oscillations for  $\mathbf{e}_i \parallel \mathbf{e}_s$  and  $\mathbf{e}_i \perp \mathbf{e}_s$  are shifted by  $45^\circ$  relative to each other which means that they are opposite in phase. Again, we note that—by using appropriate transformation matrices—this formalism can be transferred to analyze kesterite layers with an arbitrary crystal orientation, e.g.,  $\text{Cu}_2\text{ZnSnS}_4(112)$  on  $\text{Si}(111)$ .

On the other hand, for a randomly oriented ensemble of unit cells (as found in fully polycrystalline samples), no intensity oscillations are expected, since contributions from all different possible orientations average out. This fact can be used to verify that the oscillations occurring in our experiments are no measurement artifacts.

Figure 1 shows a typical normalized polarized Raman spectrum of a textured CZTSe layer on GaAs(001). For a change in the polarizer configuration, a decrease in intensity by a factor of around 4 is observed going from  $\mathbf{e}_i \parallel \mathbf{e}_s$  to  $\mathbf{e}_i \perp \mathbf{e}_s$ . The kesterite main modes at 172 and 197  $\text{cm}^{-1}$  have been reported to be of A symmetry [9] whereas the observed modes at around 249  $\text{cm}^{-1}$  have been reported to be either B- or E-modes [19, 20]. The same holds for the CZTSe mode

Table 2. Angular intensity dependencies for sample rotation around the optical axis for the different CZTSe unit cell orientations on GaAs(001).

Unit cell orientation	Symmetry	$\mathbf{e}_i \parallel \mathbf{e}_s$	$\mathbf{e}_i \perp \mathbf{e}_s$
	A	$\propto  a ^2$	0
	B	$\propto  c(\cos^2 \alpha - \sin^2 \alpha) + 2d \sin \alpha \cos \alpha ^2$	$\propto  d(\cos^2 \alpha - \sin^2 \alpha) - 2c \sin \alpha \cos \alpha ^2$
	E	0	0
	A	$\propto  a \cos^2 \alpha + b \sin^2 \alpha ^2 +  b \cos^2 \alpha + a \sin^2 \alpha ^2$	$\propto 2(a-b)^2 \cos^2 \alpha \sin^2 \alpha$
	B	$\propto c^2(\cos^4 \alpha + \sin^4 \alpha)$	$\propto 2c^2 \cos^2 \alpha \sin^2 \alpha$
	E	$\propto 4(e^2 + f^2) \cos^2 \alpha \sin^2 \alpha$	$\propto (e^2 + f^2)(\cos^2 \alpha - \sin^2 \alpha)^2$

at around  $80 \text{ cm}^{-1}$ .

However, the theoretical intensity oscillations for a sample rotation do not change qualitatively in terms of period or phase depending on the mode symmetry (B or E), since in our experiment the optical axis coincides with the highly symmetrical CZTSe directions ([001] or [100] or [010]). Besides, the scope of this article is not to accurately determine the symmetry of the occurring Raman modes but instead to detect a preferential unit cell orientation within the thin film and to judge the crystal quality.

Figure 2 shows the observed angular intensity dependence of the different samples for both the kesterite A-mode at  $197 \text{ cm}^{-1}$  and the CZTSe mode at around  $80 \text{ cm}^{-1}$ . All Raman intensities were measured in the peak maximum and normalized to the intensity of the CZTSe A-mode at  $197 \text{ cm}^{-1}$  ( $\mathbf{e}_i \parallel \mathbf{e}_s$ ). The randomly orientated polycrystalline sample does not exhibit any angular intensity dependence. Fluctuations in the signal do not exhibit any periodicity and are purely due to an inhomogeneous sample quality. This is consistent with the theoretical expectation that all contributions from randomly orientated grains average out. Furthermore, this result confirms that the observed oscillations for the other samples are not an artifact of the measurement.

In contrast to that, both the textured and the epitaxial sample exhibit a clear angular intensity dependence. For the CZTSe mode around  $80 \text{ cm}^{-1}$  an oscillation with a period of  $90^\circ$  is observed for both polarizer configurations. As expected, the oscillations are opposite in phase for the two different polarizations. These findings prove the strong preferential orientation of unit

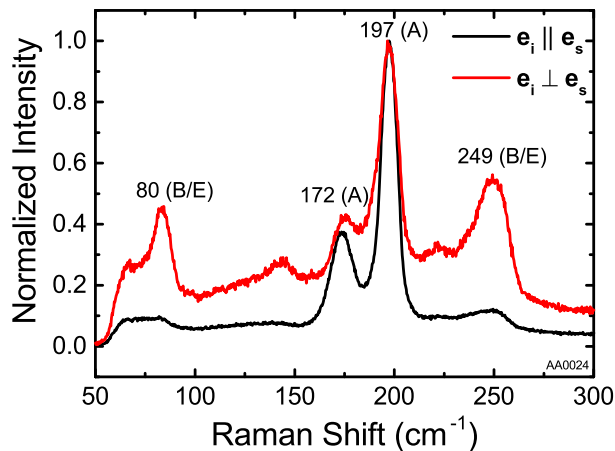


Fig. 1. Polarized Raman spectrum of a textured sample for the two possible polarizations  $\mathbf{e}_i \parallel \mathbf{e}_s$  and  $\mathbf{e}_i \perp \mathbf{e}_s$ .

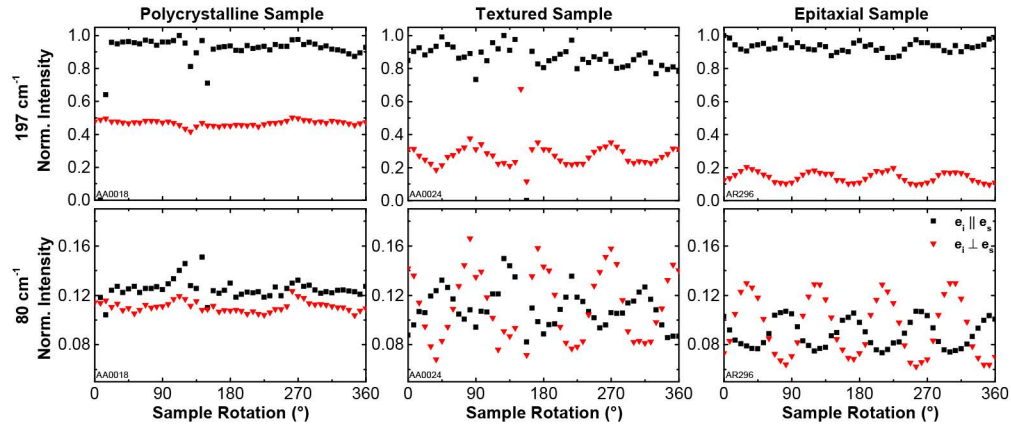


Fig. 2. Intensity dependence under sample rotation for three different samples. The polycrystalline sample does not exhibit any oscillations whereas the epitaxial samples exhibit intensity oscillations with a period of  $90^\circ$ . The intensity behaviour of the A-mode indicates the presence of lying kesterite unit cells on the GaAs substrate. Intensities were normalized to the A-mode at  $197\text{ cm}^{-1}$  ( $\mathbf{e}_i \parallel \mathbf{e}_s$ ).

cells within the sample. The kesterite modes at around  $249\text{ cm}^{-1}$  exhibit the same behaviour qualitatively under sample rotation which is why they are not shown separately in this letter.

Interestingly, for  $\mathbf{e}_i \parallel \mathbf{e}_s$  the kesterite A-modes of the textured and the epitaxial CZTSe sample show an almost constant intensity under sample rotation which is consistent with theory for standing kesterite unit cells. However, slight intensity oscillations are visible. Furthermore, for  $\mathbf{e}_i \perp \mathbf{e}_s$  we observe an intensity oscillation instead of a vanishing signal. This confirms the existence of lying kesterite unit cells within the film. We conclude that the majority of unit cells is of standing orientation on GaAs due to the constant A-mode intensity under sample rotation for  $\mathbf{e}_i \parallel \mathbf{e}_s$ . This majority of standing unit cells is then blocked out when  $\mathbf{e}_i \perp \mathbf{e}_s$ , and the remaining oscillating signal is originating from the minority of lying unit cells. For  $\mathbf{e}_i \parallel \mathbf{e}_s$  the resulting oscillation for a mixture of standing (constant intensity) and lying (oscillating intensity) unit cells is probably masked by sample inhomogeneities on the surface. In addition, an increasing contrast between the A-mode intensity for  $\mathbf{e}_i \parallel \mathbf{e}_s$  and  $\mathbf{e}_i \perp \mathbf{e}_s$  can be observed when looking at the transition in crystallinity for those three samples going from left to right in Fig. 2. One way to interpret this finding is that the amount of polycrystalline inclusions with a different grain orientation is further reduced in the epitaxial sample compared to the textured sample.

Again, the behaviour of the second A-mode at  $172\text{ cm}^{-1}$  is qualitatively identical to the Raman mode at  $197\text{ cm}^{-1}$  and is therefore not shown either. Since the presence of a stannite phase cannot be excluded within the sample it is important to note that the Raman tensor of the corresponding stannite  $A_1$ -mode is identical in shape with that of a kesterite A-mode. Accordingly, the same intensity behaviour results for the different unit cell orientations. This means that the conclusions which were drawn about the unit cell orientation also hold for stannite CZTSe on GaAs(001).

By comparing the intensity oscillations of the textured and the epitaxial sample one finds that the oscillation patterns are more homogeneous for the latter one. This can be interpreted in a way that the surface of the epitaxial sample is more homogeneous than for the textured sample. A comparison of XRD analyses such as rocking curve measurements and  $\phi$ -scans which we also used to prove the preferential grain orientation in our textured films [4] yielded a similar

crystalline orientation for both epitaxial and textured layers. This means, that—due to the finite penetration depth of the laser and the small spot size—polarized Raman spectroscopy is able to detect sample inhomogeneities with a higher spatial resolution than XRD analysis.

### **3. Conclusion**

In conclusion, Raman spectroscopy has been used to assess the crystallographic orientation in CZTSe samples. Clear intensity oscillations evolve from a constant signal under sample rotation when the unit cell order within the films is increased. This has been shown experimentally by analyzing three different types of sample crystallinities going from a randomly oriented ensemble of unit cells in a polycrystalline CZTSe layer on Mo/SLG to a textured layer and an epitaxial layer on GaAs(001). Furthermore, it has been shown that the observed intensity oscillations cannot be due to purely standing kesterite unit cells on GaAs. These findings confirm that polarized Raman spectroscopy can be used to easily access unit cell orientations within high-quality CZTSe layers and additionally grants high spatial resolution. By analyzing the intensity contrast between the different polarizer configurations it is possible to obtain information about the degree of texture by comparison of different samples. The analysis can be extended to investigate kesterite layers with an arbitrary crystal orientation to determine crystallinity and unit cell orientation.

### **Acknowledgments**

We acknowledge financial support from the Karlsruhe School of Optics and Photonics (KSOP) and funding of the Luxembourgish Fonds national de la recherche. Christoph Krämmer is pursuing his PhD with a scholarship of the Carl-Zeiss-Foundation. Furthermore, we acknowledge support by Deutsche Forschungsgemeinschaft and Open Access Publishing Fund of Karlsruhe Institute of Technology.